Organic & Biomolecular Chemistry

RSC Publishing

PAPER

View Article Online
View Journal | View Issue

A novel ratiometric emission probe for Ca^{2+} in living cells†

Cite this: *Org. Biomol. Chem.*, 2013, **11**, 503

Qiaoling Liu,[a,b] Wei Bian,[a] Heping Shi,[a] Li Fan,[a] Shaomin Shuang,[a] Chuan Dong*[a] and Martin M. F. Choi*[c]

Received 25th September 2012,
Accepted 6th November 2012

DOI: 10.1039/c2ob26888d

www.rsc.org/obc

A ratiometric fluorescent probe for Ca^{2+} based on 1,3,4-oxadiazole derivative has been designed and developed. The probe exhibits a large Stokes shift of 202 nm and a highly selective ratiometric emission response (490/582 nm) to Ca^{2+} over other metal cations. Additionally, the probe can readily reveal the changes of intracellular Ca^{2+} concentration in living human umbilical vein endothelial cells.

Published on 07 November 2012 on http://pubs.rsc.org | doi:10.1039/C2OB26888D
Downloaded by University of Science and Technology of China on 23 December 2012

Introduction

Calcium ion (Ca^{2+}) as a second intracellular messenger plays multiple crucial roles in intra- and intercellular signaling. Through the temporal and spatial fluctuations of Ca^{2+} concentrations, many different cellular processes including fertilization, proliferation, metabolism, contraction and apoptosis can be regulated.[1] The total calcium content in resting cells is generally 1–7 mM, but most of the cellular calcium (>99.9%) is stored in organelles such as mitochondria and endoplasmic reticulum. The free Ca^{2+} is only around 100 nM. However, during various cellular functions, the free Ca^{2+} concentration can be regulated by the release of Ca^{2+} from the intracellular Ca^{2+}-storing organelles and the concentration sometimes goes up 10–100 folds.[2] Thus, tracking the dynamic changes of intracellular Ca^{2+} concentration and understanding the signal Ca^{2+} pathways would certainly help us recognize many cellular processes and functions.

Up to now, a successful approach for intracellular Ca^{2+} measurement is to introduce the optically sensitive Ca^{2+} probes into living cells, combining with digital imaging microscopy. This technique possesses the advantages of high sensitivity, good selectivity, fast response time, and *in situ* observation.[3] A Ca^{2+} probe works best if its dissociation constant (K_d) is close to the intracellular Ca^{2+} concentration. When the calcium concentration is higher or is involved in fast transients, the probe with small K_d could saturate quickly and results in inaccurate measurement. On the other hand, if the K_d is too large, Ca^{2+} measurement will be insensitive.[4] So the chosen Ca^{2+} probe with an appropriate value of K_d is of great importance for accurate intracellular Ca^{2+} measurement.

In addition, in view of intensity- and ratiometric-based Ca^{2+} probes, the latter is more desirable than the former in proper detection of Ca^{2+} since ratiometric probes allow for internal calibration of Ca^{2+} and obviate the experimental corrections of photobleaching, sample thickness variability and differential loading of probe within the cell.[5] To date, only a few ratiometric Ca^{2+} probes, including Fura-2, Indo-1 and Indo-5F, are commercially available and they have been widely utilized to monitor the changes of intracellular Ca^{2+} and assisted us in recognizing some diseases such as hyperparathyroidism, tumor metastasis and renal failure.[6] It is noteworthy that these ratiometric Ca^{2+} probes all adopt 1,2-bis(2-aminophenoxy) ethane-*N*,*N*,*N*′,*N*′-tetraacetic acid (BAPTA) structure for selectively binding Ca^{2+}.[7] This type of Ca^{2+} probe ensures good sensitivity and selectivity for Ca^{2+} over other physiological metal ions. To our knowledge, in this kind of ratiometric Ca^{2+} probes, only Indo-1 and Indo-5F can perform emission ratio measurements as a function of Ca^{2+} concentration. Unfortunately, Indo-1 and Indo-5F require UV excitation which will inevitably lead to photobleaching, high scattering background and autofluorescence interference.[8] Moreover, their K_d are relatively small (0.23 and 0.47 μM, respectively) so that their applications in cells and tissues are quite limited.

In this paper, we report the development of a novel Ca^{2+} probe based on ratiometric emission measurement. Our molecular design strategy is to incorporate 2-(4-ethoxyphenyl)-5-(4-methylphenyl)-1,3,4-oxadiazole as the fluorophore and BAPTA group as the Ca^{2+} recognition site. To our knowledge, 1,3,4-oxadiazole (OXD) derivative based Ca^{2+} probe has not been reported before. Owing to the electron-deficient property of OXD, when it conjugates to the electron-rich groups of

[a]*Research Center of Environmental Science and Engineering, and School of Chemistry and Chemical Engineering, Shanxi University, Taiyuan 030006, P. R. China. E-mail: dc@sxu.edu.cn; Fax: +86-0351-7018613; Tel: +86-0351-7018613*
[b]*Department of Chemistry, Taiyuan Normal University, Taiyuan 030031, P. R. China*
[c]*Department of Chemistry, Hong Kong Baptist University, 224 Waterloo Road, Kowloon Tong, Hong Kong SAR, P. R. China. E-mail: mfchoi@hkbu.edu.hk; Fax: +852-34117348; Tel: +852-34117839*

†Electronic supplementary information (ESI) available: Determinations of dissociation constants and quantum yields, Supplementary figures, NMR spectra and mass spectrum. See DOI: 10.1039/c2ob26888d

Downloaded by University of Science and Technology of China on 23 December 2012
Published on 07 November 2012 on http://pubs.rsc.org | doi:10.1039/C2OB26888D

ethoxybenzene and salt form of BAPTA, intramolecular charge transfer (ICT) from the donor to the acceptor will proceed upon photon irradiation. This push–pull conjugated molecule will exhibit a large Stokes shift attributing to its large π-electron conjugation system. In addition, since there is an overlap of the excitation spectrum of OXD fluorophore (260–360 nm) with that of BAPTA (230–320 nm), the same excitation wavelength could be applied to trigger the emissions of OXD fluorophore and BAPTA. It is envisaged that Ca^{2+} coordination to BAPTA will alter the emission ratio of OXD fluorophore to BAPTA, offering ratiometric Ca^{2+}-sensing capability. When BAPTA binds with a Ca^{2+} ion, its electron-donating property will be restricted with a concomittant reduction of π-electron conjugation and, as a result, both absorption and emission spectra are blue-shifted, which will provide potential for Ca^{2+} detection. Furthermore, since OXD–BAPTA–ester permeates the membrane easily, OXD–BAPTA–ester loaded cells will provide an opportunity to observe the intracellular Ca^{2+} signal *in situ* by confocal microscopic imaging. The structures and color changes of OXD–BAPTA and its Ca^{2+}-complex are depicted in Scheme 1.

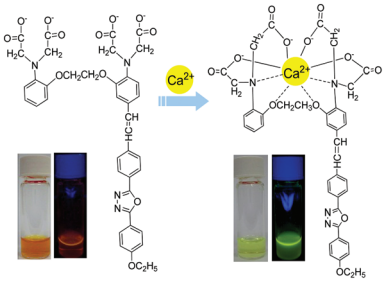

Scheme 1 The structures of OXD–BAPTA and its Ca^{2+}-complex with color changes.

Results and discussion

Synthetic routes of OXD–BAPTA–ester and OXD–BAPTA are depicted in Scheme 2, compound **1** (2-(4-ethoxyphenyl)-5-(4-methylphenyl)-1,3,4-oxadiazole) and compound **2** (2-[(4-bromomethyl)phenyl]-5-(4-ethoxyphenyl)-1,3,4-oxadiazole) were prepared according to previous reports with slight modifications.[9] Compound **3** (5-formyl-BAPTA-tetraethyl ester) was obtained by following the Grynkiewicz *et al.* method.[10] Compound **2** and **3** were coupled by the Wittig reaction under N_2 atmosphere and subsequently purified by column chromatography to obtain the yellow solid OXD–BAPTA–ester in 60% yield. OXD–BAPTA was obtained by base hydrolysis of OXD–BAPTA–ester in aqueous lithium hydroxide, and the OXD–BAPTA–ester was fully characterized by ^{1}H NMR, ^{13}C NMR, mass spectrum and elemental analyses (ESI†).

The absorption spectral change of OXD–BAPTA in HEPES buffer solution (50 mM, pH 7.2) in the presence of various concentrations of Ca^{2+} ion are displayed in Fig. 1. Free OXD–BAPTA shows two strong absorption bands centered at 305 nm (ε = 3.43 × 10^4 M^{-1} cm^{-1}) and 380 nm (ε = 4.46 × 10^4 M^{-1} cm^{-1}), assigned to the π–π* transition and ICT bands, respectively. On the addition of Ca^{2+} (0.0–11.1 μM) to the 10.0 μM OXD–BAPTA solution, the bands at 305 and 380 nm decrease gradually and the ICT band exhibits a large hypsochromic shift to 350 nm with the solution changing color from orange to faint greenish yellow (Inset of Fig. 1).

Fig. 2 depicts the fluorescence emission spectral changes of OXD–BAPTA after the addition of Ca^{2+} ion under physiological conditions. At an excitation wavelength of 380 nm (Fig. 2a), a strong emission band with a fluorescence emission maximum (λ^{fl}_{max}) of 582 nm is observed, corresponding to the free OXD–BAPTA. On addition of Ca^{2+} to OXDA–BAPTA, the λ^{fl}_{max} shifts from 582 to 490 nm. An isoemissive point of 518 nm is clearly found, indicating the formation of OXD–BAPTA–Ca^{2+} complex. A similar result is obtained at the excitation wavelength of

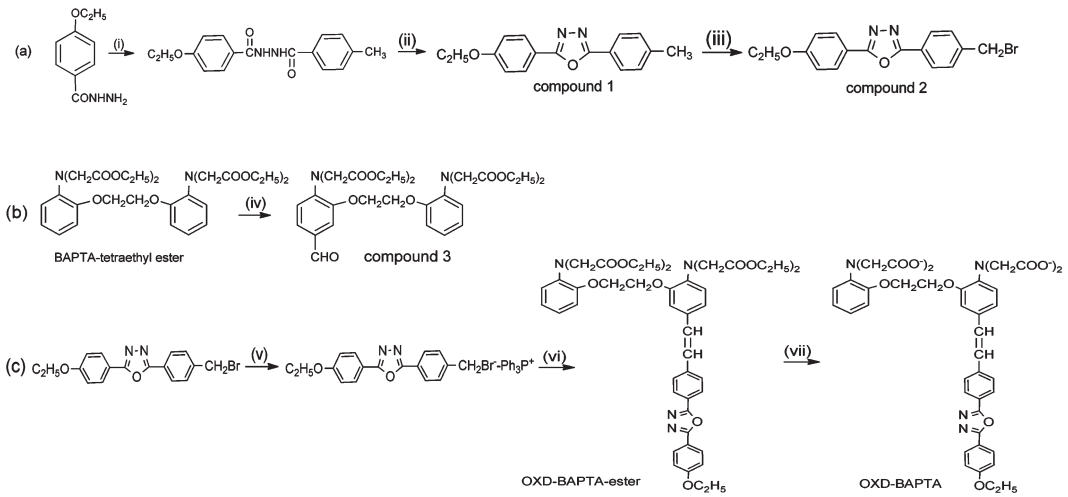

Scheme 2 Synthetic procedures of OXD–BAPTA. *Conditions*: (a) (i) *p*-Toluoyl chloride, py, reflux 3 h, 90%; (ii) $POCl_3$, reflux 7 h, 60%; (iii) NBS, reflux 5 h, 90%; (b) (iv) $POCl_3$, DMF, 54%; (c) (v) Ph_3P; (vi) NaH, compound **3**, 60% (vii) LiOH, 97%.

 This journal is © The Royal Society of Chemistry 2013

Downloaded by University of Science and Technology of China on 23 December 2012
Published on 07 November 2012 on http://pubs.rsc.org | doi:10.1039/C2OB26888D

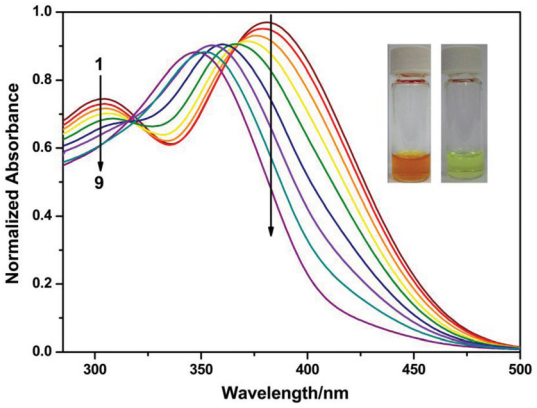

Fig. 1 Absorption spectra of 10.0 μM OXD–BAPTA in 50 mM HEPES (pH 7.2) containing 100 mM KCl and 10 mM EGTA in the presence of various concentrations of Ca^{2+} ions (1–9: 0.00, 0.038, 0.098, 0.227, 0.341, 0.582, 0.906, 2.04, and 11.1 μM). EGTA stands for ethylene glycol bis(β-aminoethyl ether)-*N*,*N*,*N*′,*N*′-tetraacetic acid. The inset shows the images of OXD–BAPTA before (left) and after (right) addition of Ca^{2+}.

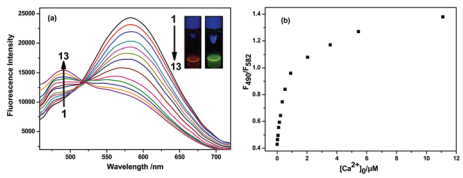

Fig. 2 (a) Fluorescence emission spectra of 1.0 μM OXD–BAPTA in 50 mM HEPES (pH 7.2) containing 100 mM KCl and 10 mM EGTA in the presence of various concentrations of Ca^{2+} ions (1–13): 0.00, 0.026, 0.038, 0.098, 0.15, 0.227, 0.341, 0.582, 0.906, 2.04, 3.56, 5.45, and 11.1 μM at excitation wavelengths of 380 nm. The inset shows the fluorescence emission images of OXD–BAPTA before (left) and after (right) addition of Ca^{2+} under UV lamp irradiation. (b) Ratiometric calibration curve F_{490}/F_{582} as a function of Ca^{2+} concentration.

350 nm. Accordingly, the fluorescence color changes from pale red to bright green under irradiation of an UV lamp (Inset of Fig. 2a). The ratio of fluorescence intensity F_{490}/F_{582} also changes linearly with the concentration of Ca^{2+} (Fig. 2b), this result suggests that OXD–BAPTA can be used as a good ratiometric probe.

The absorption and emission spectral properties illustrate that Ca^{2+} ion binds to the BAPTA moiety of OXD–BAPTA so as to weaken the ability of BAPTA to participate in the π-electron conjugation of the molecule. Thus, the π-electron density in the conjugated molecule decreases, resulting in reduction of ICT. On the whole, both absorption and emission bands are blue-shifted. The spectrofluorometric data also provide us valuable information for exploring the potential application of OXD–BAPTA for determination of intracellular Ca^{2+} since there is a large Stokes shift of 202 nm between the excitation (380 nm) and emission (582 nm) peaks. This can minimize spectral interference from the excitation light beam and autofluorescence. Moreover, a large spectral shift (92 nm) between the two λ_{max}^{fl} (490 and 582 nm) and their changes in emission intensity result in a huge ratiometric value (Fig. 2a and 2b).

Table 1 Spectra properties of ratiometric emission Ca^{2+} probes

Probe	E_x (nm)	E_m (nm)	Stokes shift (nm)	K_d (μM)
Indo-1[a]	346	401/475	129	0.23
Indo-5F[a]	344	398/471	127	0.47
OXD–BAPTA[b]	380	490/582	202	0.56 ± 0.08

Spectra data and K_d values measured in 100 mM KCl, 10 mM EGTA and (a) 10 mM MOPS or (b) 50 mM HEPES at pH 7.20.

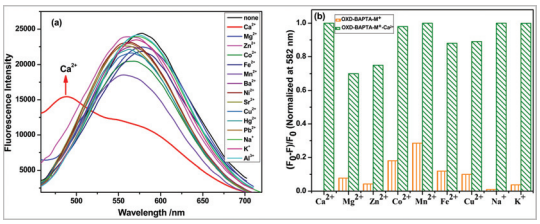

Fig. 3 (a) The fluorescence spectra of 1.0 μM OXD–BAPTA in the presence of 11.1 μM Ca^{2+}, 150 μM Mg^{2+}, Zn^{2+}, Co^{2+}, Mn^{2+}, Fe^{2+}, Cu^{2+}, Ba^{2+}, Ni^{2+}, Sr^{2+}, Hg^{2+}, Pb^{2+}, Na^+, K^+ and Al^{3+} in 50 mM HEPES (pH 7.2) containing 100 mM KCl. (b) Relative fluorescence intensity of 1.0 μM OXD–BAPTA in the presence of 150 μM Mg^{2+}, Zn^{2+}, Co^{2+}, Mn^{2+}, Fe^{2+}, Cu^{2+}, Na^+ and K^+ (orange bars) followed by addition of 11.1 μM Ca^{2+} (olive bars) in 50 mM HEPES (pH 7.2) containing 100 mM KCl. F_o and F are the fluorescence intensities of OXD–BAPTA in the absence and presence of metal ions, respectively. The excitation wavelength is 380 nm.

The stoichiometric ratio for the formation of OXD–BAPTA–Ca^{2+} complex was determined by the Job's method and the result indicates the formation of OXD–BAPTA–Ca^{2+} complex with a 1 : 1 ratio of OXD–BAPTA to Ca^{2+} (Fig. 1S, ESI†). The dissociation constant (K_d) of OXD–BAPTA–Ca^{2+} complex was determined as 0.56 ± 0.080 μM (Fig. 2S, ESI†), suggesting that the dissociation constant is relatively small, but larger than that of Indo-1 and Indo-5F (Table 1). Thus, OXD–BAPTA could bind to Ca^{2+} with good stability. The spectral response of OXD–BAPTA toward Mg^{2+} was also studied (Fig. 3S, ESI†). The emission spectra show that OXD–BAPTA for Mg^{2+} is only an intensity-based probe and the OXD–BAPTA–Mg^{2+} complex is formed the 1 : 1 ratio of OXD–BAPTA to Mg^{2+} which is determined by the Hill plot. The K_d for OXD–BAPTA–Mg^{2+} is 4.35 ± 0.075 mM, suggesting the affinity of OXD–BAPTA to Mg^{2+} is much smaller than that of Ca^{2+}.

The fluorescence spectra of OXD–BAPTA with various metal cations are described in Fig. 3a. Among these metal ions, Ca^{2+} exhibits the largest effect on the fluorescence intensity of OXD–BAPTA. Fig. 3b displays the normalized relative response of OXD–BAPTA to the physiological metal ions. Mn^{2+} and Co^{2+} show moderate effect while Fe^{2+}, Mg^{2+}, Zn^{2+}, Cu^{2+}, Na^+ and K^+ have slight effect on the fluorescence intensity of OXD–BAPTA. Fortunately, the intracellular concentrations of free Mn^{2+} and Co^{2+} ions are negligible. In addition, OXD–BAPTA shows good response to Ca^{2+} when both Ca^{2+} and the physiological metal ions are co-existed in the HEPES buffer solution, indicating

Downloaded by University of Science and Technology of China on 23 December 2012
Published on 07 November 2012 on http://pubs.rsc.org | doi:10.1039/C2OB26888D

that OXD–BAPTA displays excellent selectivity for Ca^{2+} over other physiological cations so that OXD–BAPTA could be employed to measure the intracellular free Ca^{2+}. Furthermore, the pH effect on OXD–BAPTA in the biologically relevant pH range determines that the optimal condition is pH 7.0–7.5 (Fig. 4S, ESI†).

The fluorescence quantum yields (Φ) of OXD–BAPTA and OXD–BAPTA–Ca^{2+} complex were determined as 0.007 and 0.010 at an excitation wavelength of 350 nm; 0.022 and 0.017 at excitation wavelength of 380 nm, respectively. Quinine bisulfate in 0.050 M H_2SO_4 (Φ of 0.546) was used as the fluorescence standard (ESI†). The small Φ is attributed to the polar solvent of water. Polar solvent–solute interactions lead to a reduced coplanar effect, more efficient nonradiative deactivation and finally lead to a drastically reduced brightness.[11] For the OXD–BAPTA–Ca^{2+} complex, Ca^{2+}-binding induces a reduction of ICT which in turn results in a smaller Φ. The fluorescence lifetime (τ) for OXD–BAPTA and OXD–BAPTA–Ca^{2+} were determined from time-resolved fluorescence spectroscopy as 1.52 and 1.51 ns at excitation wavelength of 350 nm; 1.16 and 1.15 ns at excitation wavelength of 380 nm, respectively.

To explore the potential application of OXD–BAPTA in living cell imaging and the dynamic change of intracellular Ca^{2+} signal, OXD–BAPTA–ester was employed for cell permeability. Human umbilical vein endothelial cells (HUVEC) were incubated with OXD–BAPTA–ester (5.0 μM) for 40 min at 37 °C, and then the ester was converted to the active form of OXD–BAPTA inside the cells by intracellular esterase, which ensured the Ca^{2+} signal could be deciphered in the cytosol. Prior to imaging, the medium was removed, and the OXD–BAPTA stained HUVEC were washed with HEPES three times.[12] Confocal fluorescent imaging was performed at an excitation wavelength of 458 nm since 380 nm laser was not available for the confocal microscope, the emission wavelengths were centered at 580 ± 20 nm and 490 ± 20 nm for the fluorescent properties of OXD–BAPTA and its Ca^{2+}-complex. Fig. 4a and 4b depict images of the stained cells with bright red and faint green fluorescence at the above-mentioned emission wavelengths, indicating a lower free Ca^{2+} concentration in cytosol as the resting levels of $[Ca^{2+}]_i$. Then these OXD–BAPTA stained cells were given to penicillin G sodium salt (30 U mL^{-1}), the cell images were captured again after 180 s as depicted in Fig. 4c and 4d. The red fluorescence drops dramatically and the green fluorescence was enhanced, inferring the release of $[Ca^{2+}]_i$ from the intracellular Ca^{2+}-storing organelles after administration of penicillin G sodium salt. Fig. 4e records the changes of the fluorescence intensities at the marked circle areas 1 and 2 for 180 s at the above-mentioned emission wavelengths. Fig. 4f exhibits the ratiometric change F_{490}/F_{582} for 180 s. These results indicate that the intracellular $[Ca^{2+}]_i$ can be determined in real-time after the living cells have been exposed to the irritation of drugs. In essence, OXD–BAPTA is obviously capable of visualizing the intracellular $[Ca^{2+}]_i$ waves in living cells under a confocal laser scanning microscope.

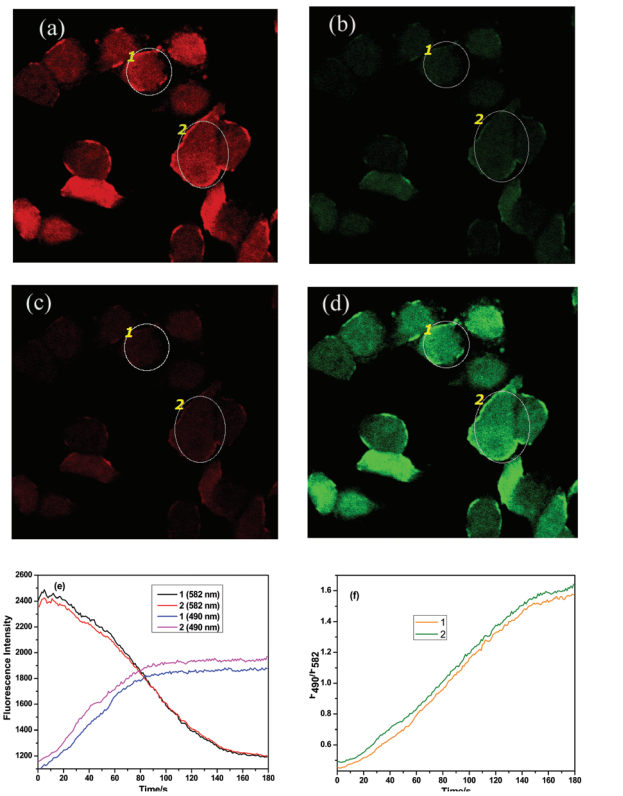

Fig. 4 Confocal fluorescence images of intracellular Ca^{2+} in living HUVEC. The excitation wavelength is 458 nm, the emission wavelengths are centered at 580 ± 20 nm and 490 ± 20 nm (20 × objective lens). (a), (b) HUVEC are incubated with 5.0 μM OXD–BAPTA for 40 min at 37 °C, observing emission wavelengths at 580 ± 20 nm and 490 ± 20 nm, respectively. (c), (d) Penicillin G sodium salt (30 U mL^{-1}) is added to the OXD–BAPTA stained HUVEC. The images are captured after 180 s at emission wavelengths of 580 ± 20 nm and 490 ± 20 nm, respectively. (e) Fluorescence intensities are recorded at the marked circle areas 1 and 2 from (a) to (c) and (b) to (d) for 180 s at emission wavelengths of 580 ± 20 nm and 490 ± 20 nm, respectively. (f) Ratiometric fluorescence change F_{490}/F_{582} for 180 s.

Conclusions

In summary, we have developed an emission ratiometric probe (OXD–BAPTA) for detecting intracellular $[Ca^{2+}]_i$. The main attributes of this probe are that it displays high sensitivity and selectivity for Ca^{2+} over other metal ions, a large Stokes shift of 202 nm and enables ratiometric emission measurement with an obvious color change. Moreover, OXD–BAPTA can track the $[Ca^{2+}]_i$ signal in real-time in living HUVEC by microscopic imaging. These special traits indicate that OXD–BAPTA is an excellent probe for intracellular Ca^{2+} signal.

Experimental section

Materials and characterization

All chemicals were purchased from Shanghai Aladdin Reagent Co., Ltd. Organic solvents (AR grade) were purchased from commercial suppliers without further purification before use. Deionized water was obtained from a Milli-Q water purification

 This journal is © The Royal Society of Chemistry 2013

Published on 07 November 2012 on http://pubs.rsc.org | doi:10.1039/C2OB26888D
Downloaded by University of Science and Technology of China on 23 December 2012

system (Millipore). 50 mM HEPES buffer solution (pH 7.2) containing 100 mM KCl and 10 mM EGTA was used to prepare the OXD–BAPTA solutions. The stock solutions of 1.0 mM OXD–BAPTA–ester were prepared by dissolving OXD–BAPTA–ester in dimethyl sulfoxide and kept at −18 °C. 0.20 M stock solutions of Ca^{2+}, Mg^{2+}, Zn^{2+}, Co^{2+}, Mn^{2+}, Fe^{2+}, Cu^{2+}, Ba^{2+}, Ni^{2+}, Sr^{2+}, Hg^{2+}, Pb^{2+}, Na^{+}, K^{+} and Al^{3+} were prepared from their chloride salts. 0.20 M Fe^{2+} solution and 1500 U mL^{-1} penicillin G sodium salt were freshly prepared just before experiments. UV-vis absorption spectra were recorded on a Puxi TU-1901 UV-vis absorption spectrophotometer (China). ^{1}H NMR spectra and ^{13}C NMR were recorded on a Bruker AVANCE III 600 NMR spectrometer (Germany). Elemental analysis was conducted on an Elementar Vario EL Cube CHNOS analyzer (Germany). Mass spectrum was acquired on a Bruker Autoflex matrix-assisted laser desorption/ionization time of flight (MALDI-TOF) mass spectrometer (Germany). Steady-state fluorescence measurements were performed on an Edinburgh FLSP 920 spectrofluorometer (UK) at 21 ± 1 °C.

Cell culture and imaging

Human umbilical vein endothelial cells (HUVEC) were cultured in DEME supplemented with 10% FCS (Invitrogen). One day before cell imaging, HUVEC were seeded on cover slips. The next day, HUVEC were incubated with 5.0 μM OXD–BAPTA–ester for 40 min at 37 °C under 5% CO_2, washed with HEPES buffer three times and then subjected to cell imaging under an Olympus FluoView 1000 confocal laser scanning microscope using an objective lens (20×) and an excitation light beam of 458 nm. The fluorescence intensity was recorded. Next, 30 U mL^{-1} penicillin G sodium salt was added to these OXD–BAPTA–ester incubated cells and simultaneously recorded the change of intracellular Ca^{2+} signal ($[Ca^{2+}]_i$) within 180 s. For all imaging, the microscope settings such as brightness, contrast, and exposure time were held constant to compare the changes in the fluorescent intensities of incubated cells with or without penicillin G sodium salt.

Synthesis of 2-(4-ethoxyphenyl)-5-(4-methyl phenyl)-1,3,4-oxadiazole (1)

4-Methylbenzyol chloride was initially prepared by reacting 4-methylbenzoic acid (1.81 g, 13.3 mmol) with 2 mL thionyl chloride under reflux for 3 h. The reaction mixture was concentrated under reduced pressure to give the crude acid chloride yellow solution. It was then gradually added to 10 mL $CHCl_3$ containing 4-ethoxybenzhydrazide (2.18 g, 12.1 mmol) and 1.1 mL pyridine. The mixture was stirred under reflux for 3 h and concentrated under reduced pressure. The residue was washed with water and recrystallized from hot ethanol; a white crystalline powder was obtained (3.24 g, 90%) and dried in vacuum. The dried white crystalline powder was heated in 10 mL $POCl_3$ under reflux for 7 h. The solution was concentrated under reduced pressure to give the crude solid product. After cooling to room temperature, the precipitate was washed with ice water. An aqueous solution of sodium acetate (50% w/w) was added and the precipitate was extracted twice with ethyl acetate. The combined organic extracts were concentrated under reduced pressure to obtain compound **1** (1.47 g, 60% yield) as faint yellow crystalline powder. Melting point: 129–132 °C. ^{1}H NMR (600 MHz, $CDCl_3$): δ 8.00 (d, Ar–H, 2H), 7.91 (d, Ar–H, 2H), 7.30 (d, Ar–H, 2H), 7.05 (d, Ar–H, 2H), 4.10 (q, $-CH_2-$, 2H), 2.34 (s, CH_3-, 3H), and 1.32 (t, CH_3-, 3H).

Synthesis of 2-[(4-bromomethyl)phenyl]-5-(4-ethoxyphenyl)-1,3,4-oxadiazole (2)

Compound **1** (1.47 g, 5.0 mmol), *N*-bromosuccinimide (0.95 g, 5.0 mmol) and 0.015 g benzoyl peroxide were dissolved in 12 mL dry benzene. The mixture solution was stirred and heated to reflux for 5 h. Benzene was removed on a rotary evaporator and the precipitate was recrystallized from hot ethanol to obtain 2-[(4-bromomethyl)phenyl]-5-(4-ethoxyphenyl)-1,3,4-oxadiazole (**2**, 1.70 g, 90% yield) as yellow crystalline powder. Melting point: 104–108 °C. ^{1}H NMR (600 MHz, $CDCl_3$): δ 8.00 (d, Ar–H, 2H), 7.95 (d, Ar–H, 2H), 7.30 (d, Ar–H, 2H), 7.05 (d, Ar–H, 2H), 4.10 (q, $-CH_2-$, 2H), 4.60 (s, $-CH_2-$, 2H), and 1.32 (t, CH_3-, 3H).

Synthesis of 5-formyl-BAPTA-tetraethyl ester (3)

5-Formyl-BAPTA-tetraethyl ester (**3**) was synthesized following the Grynkiewicz *et al.* method.[10] 16 mL phosphorus oxychloride was added dropwise to the solution of BAPTA–tetraethyl ester (6.0 g, 10.2 mmol) in 30 mL dry DMF and 21 mL dry pyridine at 0 °C. The reaction mixture was stirred for 30 min at room temperature, followed for 1 h at 70 °C and overnight at room temperature. Then 100 mL chloroform was added to extract twice the product. This extracted solution was washed with ice water to neutral and dried over Na_2SO_4. The filtrate was removed under reduced pressure and concentrated under reduced pressure. This concentrated solution was purified by column chromatography using silica gel as the stationary phase and ether/ethyl acetate (1 : 1) as the eluent to obtain 3.41 g (54% yield) white powder. ^{1}H NMR (600 MHz, $CDCl_3$): δ 9.63 (s, –CHO, 1H), 7.51 (d, Ar–H, 1H), 7.30 (d, Ar–H, 1H), 6.88 (dd, Ar–H, 2H), 6.65 (d, Ar–H, 2H), 6.38 (d, Ar–H, 1H), 4.58(s, $-CH_2-CH_2-$, 4H), 4.32 (s, $-CH_2-$, 8H), 4.12 (q, $-CH_2-$, 8H), and 1.32 (t, CH_3-, 12H).

Synthesis of OXD–BAPTA–ester

Compound **2** (1.70 g, 4.73 mmol) and triphenylphosphine (1.36 g, 4.89 mmol) were added to 25 ml dry benzene and the mixture was heated under reflux for 4 h. After cooling to room temperature, the reaction mixture was filtered to obtain the white solid phosphorane ylide and dried in vacuum (2.9 g, 4.67 mmol). Sodium hydride (0.16 g, 4.0 mmol) was put into 5 mL of petroleum ether under N_2 atmosphere and stirred for 20 min. The petroleum ether was discarded and replaced with 15 mL dried CH_2Cl_2. Phosphorane ylide (2.0 g, 3.24 mmol) was added and stirred at room temperature for 1 h. Compound **3** (2.0 g, 3.24 mmol) was loaded into the mixture and stirred at room temperature for 4 h. The mixture was concentrated and purified by column chromatography using silica gel as the stationary phase and *n*-hexane/ethyl acetate (1 : 1) as the eluent

Downloaded by University of Science and Technology of China on 23 December 2012
Published on 07 November 2012 on http://pubs.rsc.org | doi:10.1039/C2OB26888D

to obtain the yellow solid OXD–BAPTA–ester (1.7 g, 60% yield). Melting point: 62–64 °C. ^{1}H NMR (600 MHz, $CDCl_3$): δ 8.04 (d, Ar–H, 2H), 7.82 (d, Ar–H, 2H), 7.56 (d, Ar–H, 2H), 7.38 (d, Ar–H, H), 7.30 (d, Ar–H, H), 7.04 (d, Ar–H, 3H), 6.91 (s, Ar–H, 1H), 6.80 (dd, Ar–H, 1H), 6.66 (dd, 1H and d, 1H), 6.96 (d, –CH=CH–, 2H), 4.60 (s, $-CH_2-CH_2-$, 4H), 4.31 (s, $-CH_2-$, 8H), 4.12(q, $-CH_2-$.10H), and 1.31 (t, CH_3-, 15H). ^{13}C NMR (600 MHz, $CDCl_3$): δ 171, 170, 164, 161, 145, 132, 128.6, 127, 126.8, 126.7, 125.5, 121, 118, 116, 114, 110, 67, 65.5, 61.2, 61.1, 14.7 and 14.0. MALDI–TOF MS: *m*/*z* calculated for $C_{48}H_{54}N_4O_{12}^+$: 878; found: 901.5798 (M + Na^+). Elemental analysis calculated for $C_{48}H_{54}N_4O_{12}$: C 65.59, H 6.19, N 6.37, and O 21.84%; found: C 65.78, H 6.20, N 6.39, and O, 21.89%.

Synthesis of OXD–BAPTA

OXD–BAPTA was obtained by hydrolyzing OXD–BAPTA–ester in 0.50 M LiOH solution in an ice bath for 3 h. After hydrolysis, the pH was adjusted to 2–3 by dropwise addition of 1.0 M HCl with stirring. A pale yellow precipitate was collected by filtration and washed with 3 mL ice-water three times. The precipitate was put into the equivalent LiOH solution and stirred at 0 °C. Finally, the purified OXD–BAPTA product was dried in vacuum and kept at −18 °C until further use.

Acknowledgements

This work was supported by grants from the National Natural Science Foundation of China (21175086 and 21175087), and the Hundred Talent Programme of Shanxi Province, Shanxi International S&T Cooperation Program of China (2011081017).

Notes and references

1 (*a*) M. J. Berridge, M. D. Bottman and P. Lipp, *Nature*, 1998, **395**, 645; (*b*) W. Capoen, J. Sun, D. Wysham, M. S. Otegui, M. Venkateshwaran, S. Hirsch, H. Miwa, J. A. Downie, R. J. Morris, J. M. Ané and G. E. D. Oldroyd, *Proc. Natl. Acad. Sci. U. S. A.*, 2011, **108**, 14348; (*c*) M. Nedergaard and A. Verkhratsky, *Cell Calcium*, 2010, **47**, 101; (*d*) N. Steinckwich, V. Schenten, C. Melchior, S. Bréchard and E. J. Tschirhart, *J. Immunol.*, 2011, **186**, 2182.

2 (*a*) D. Si, T. Epstein, Y. E. Lee and R. Kopelman, *Anal. Chem.*, 2012, **84**, 978; (*b*) S. de la Fuente, P. Montenegro, R. I. Fonteriz, A. Moreno, C. D. Lobatón, M. Montero and J. Alvarez, *Biochim. Biophys. Acta, Bioenerg.*, 2010, **1797**, 1727.

3 (*a*) R. D. Burgoyne, *Nat. Rev. Neurosci.*, 2007, **8**, 182; (*b*) P. Vito, E. Lacana and L. D'Aamio, *Science*, 1996, **271**, 521; (*c*) A. Demuro, M. Smith and I. Parker, *J. Cell Biol.*, 2011, **195**, 515; (*d*) D. J. Rowlands, M. N. Islam, S. R. Das, A. Huertas, S. K. Quadri, K. Horiuchi, N. Inamdar, M. T. Emin, J. Lindert, V. S. Ten, S. Bhattacharya and J. Bhattacharya, *J. Clin. Invest.*, 2011, **121**, 1986.

4 (*a*) M. K. Park, A. V. Tepikin and O. H. Petersen, *Pfluegers Arch.*, 2002, **444**, 305; (*b*) R. E. Loy, M. Orynbayev, L. Xu, Z. Andronache, S. Apostol, E. Zvaritch, D. H. Maclennan, G. Meissner, W. Melzer and R. T. Dirksen, *J. Gen. Physiol.*, 2011, **137**, 43; (*c*) U. Lalo, A. Verkhratsky and Y. Pankratov, *Semin. Cell Dev. Biol.*, 2011, **22**, 220; (*d*) E. N. Dedkova and L. A. Blatter, *J. Mol. Cell Cardiol.*, 2012, **52**, 48.

5 (*a*) M. Nakano, H. Imamura, T. Nagai and H. Noji, *ACS Chem. Biol.*, 2011, **6**, 709; (*b*) L. I. Kazakova, L. I. Shabarchina and G. B. Sukhorukov, *Phys. Chem. Chem. Phys.*, 2011, **13**, 11110; (*c*) H. H. Wang, L. Xue and H. Jiang, *Org. Lett.*, 2011, **13**, 3844.

6 (*a*) Y. Okamoto, M. Takano, T. Ohba and K. Ono, *J. Mol. Cell. Cardiol.*, 2012, **52**, 988; (*b*) K. Satoh, T. Matsu-ura, M. Enomoto, H. Nakamura, T. Michikawa and K. Mikoshiba, *J. Biol. Chem.*, 2011, **286**, 20591; (*c*) D. S. Adams and M. Levin, *Cold Spring Harb. Protoc.*, 2012, **4**, 385; (*d*) T. P. Collins, R. Bayliss, G. C. Churchill, A. Galione and D. A. Terrar, *Cell Calcium*, 2011, **50**, 449; (*e*) Y. Ding, H.-w. Ai, H. Hoi and R. E. Campbell, *Anal. Chem.*, 2011, **83**, 9687; (*f*) J. Zou, A. M. Hofer, M. M. Lurtz, G. Gadda, A. L. Ellis, N. Chen, Y. Huang, A. Holder, Y. Ye, C. F. Louis, K. Welshhans, V. Rehder and J. J. Yang, *Biochemistry*, 2007, **46**, 12275.

7 R. Y. Tsien, *Biochemistry*, 1980, **19**, 2396.

8 (*a*) K. Y. Pu, K. Li, X. Zhang and B. Liu, *Adv. Mater.*, 2010, **22**, 4186; (*b*) K. J. Buckler, *Pfluegers Arch.*, 2012, **463**, 743; (*c*) T. P. Collins and D. A. Terrar, *J. Physiol.*, 2012, **590**, 1881.

9 (*a*) G. H. Liu, P. Yang, W. L. Jiang, X. Z. Guo, G. B. Xu, X. Z. Jiang, L. Shen and Y. M. Wang, *J. Funct. Mater.*, 2005, **36**, 600; (*b*) X. Z. Guo, X. M. Wang, Y. K. Du, N. P. Hua, M. Shen, W. L. Jiang and P. Yang, *Chin. Chem. Lett.*, 2005, **16**, 597; (*c*) X. Zhan, Y. Liu, X. Wu, S. Wang and D. Zhu, *Macromolecules*, 2002, **35**, 2529.

10 G. Grynkiewicz, M. Poenie and R. Y. Tsien, *J. Biol. Chem.*, 1985, **260**, 3440.

11 S. Sumalekshmy, M. M. Henary, N. Siegel, P. V. Lawson, Y. Wu, K. Schmidt, J. L. Brédas, J. W. Perry and C. J. Fahrni, *J. Am. Chem. Soc.*, 2007, **129**, 11888.

12 (*a*) A. M. B. Reeves, E. Shigetomi and B. S. Khakh, *J. Neurosci.*, 2011, **31**, 9353; (*b*) M. Kamiya and K. Johnsson, *Anal. Chem.*, 2010, **82**, 6472; (*c*) M. Collot, C. Loukou, A. V. Yakovlev, C. D. Wilms, D. Li, A. Evrard, A. Zamaleeva, L. Bourdieu, J.-F. Léger, N. Ropert, J. Eilers, M. Oheim, A. Feltz and J.-M. Mallet, *J. Am. Chem. Soc.*, 2012, **134**, 14923.

 This journal is © The Royal Society of Chemistry 2013